Inorg. Chem. **2004**, *43*, 5635–5644

Electrocatalytic Proton Reduction by Phosphido-Bridged Diiron Carbonyl Compounds: Distant Relations to the H-Cluster?

Mun Hon Cheah, Stacey J. Borg, Mark I. Bondin, and Stephen P. Best*

School of Chemistry, University of Melbourne, Victoria 3010, Australia

Received February 27, 2004

Intermediates formed during reduction of $Fe_2(\mu\text{-}PPh_2)_2(CO)_6$ (**1**) in the presence of protons have been identified by spectroelectrochemical, continuous-flow, and interrupted-flow techniques. The mechanism for electrocatalytic proton reduction suggested by these observations yields digital simulation of the voltammetry in close agreement with measurements conducted in THF over a range of acid concentrations. The mechanism for electrocatalytic proton reduction involves initial formation of the dianion, $\mathbf{1}^{2-}$, which is doubly protonated prior to further reduction and dihydrogen elimination. The IR spectra of the singly and doubly protonated forms of $\mathbf{1}^{2-}$ indicate structures corresponding to $[FeH(CO)_3(\mu\text{-}PPh_2)_2Fe(CO)_3]^-$ ($\mathbf{1H}^-$) and $FeH(CO)_3(\mu\text{-}PPh_2)_2FeH(CO)_3$ ($\mathbf{1H_2}$). The thiolato and dithiolato analogues of **1** exhibit electrocatalytic proton reduction associated with the two-electron reduction step, and this implies that the corresponding two-electron reduced doubly protonated species is unstable with respect to dihydrogen elimination. The stability of $\mathbf{1H_2}$ is most likely to be due to the weak interactions between the iron centers of the flattened {2Fe2P} core. Whereas $\mathbf{1H_2}$ is stable in the absence of a reducing potential, $\mathbf{1H}^-$ rearranges rapidly to a product previously described as $[Fe_2(\mu\text{-}PPh_2)(\mu\text{-}CO)(PHPh_2)(CO)_5]^-$ ($\mathbf{1H}^-_\mathbf{w}$). Another protonation product of $\mathbf{1}^{2-}$, previously formulated as $[Fe_2(\mu\text{-}PPh_2)_2(\mu\text{-}CO)H(CO)_5]^-$, has been reformulated as $[Fe_2(\mu\text{-}PPh_2)(\mu\text{-}CO)(CO)_6]^-$ (**2**) on the basis of a range of spectroscopic measurements. Solution EXAFS measurements of **1**, $\mathbf{1}^{2-}$, $\mathbf{1H}^-_\mathbf{w}$, and **2** are reported, and these yield model-independent Fe–Fe distances of 2.61 (**1**), 3.58 ($\mathbf{1}^{2-}$), 2.58 ($\mathbf{1H}^-_\mathbf{w}$), and 2.59 Å (**2**). The presence of an Fe–Fe bond for both $\mathbf{1H}^-_\mathbf{w}$ and **2** is a key aspect of the proposed structures, and this strongly supports the deductions based on spectroscopic evidence. The fits of the solution EXAFS to different structural models give statistics in agreement with the proposed structures.

Introduction

The structure of the {2Fe2S} subsite of the H-cluster of the [Fe]-hydrogenase enzyme, $\{2Fe2S\}_H$,[1] has provided a stimulus for a more intimate understanding of the chemistry of diiron carbonyl/cyanide compounds[2,3] and raised their profile as functional models of the enzyme[3−6] and potential abiological hydrogen activation catalysts. In this spirit we have been drawn into the examination of dithiolato-bridged diiron carbonyl compounds and in this investigation into the chemistry of the related phosphido-bridged diiron carbonyl compounds. The reasons that lead us to move from the more biologically relevant dithiolato-bridged compounds center on the report of a protonation product of $[Fe_2(\mu\text{-}PPh_2)_2(CO)_6]^{2-}$, $\mathbf{1}^{2-}$, that exhibits hydridic chemistry and has a proposed structure (**C**, Scheme 1) that includes both terminal hydride and bridging carbonyl ligands.[7] Moreover, the mechanistic

* Author to whom correspondence should be addressed. E-mail: spbest@unimelb.edu.au. Fax: 61-3-93805187.

(1) Peters, J. W.; Lanzilotta, W. N.; Lemon, B. J.; Seefeldt, L. C. *Science* **1998**, *282*, 1853−1858. Nicolet, Y.; Piras, C.; Legrand, P.; Hatchikian, C. E.; Fontecilla-Camps, J. C. *Structure* **1999**, *7*, 13−23.

(2) Lyon, E. J.; Georgakaki, I. P.; Reibenspies, J. H.; Darensbourg, M. Y. *Angew Chem., Int. Ed.* **1999**, *38*, 3178−3180. Schmidt, M.; Contakes, S. M.; Rauchfuss, T. B. *J. Am. Chem. Soc.* **1999**, *121*, 9736−9737. Liaw, W.-F.; Lee, N.-H.; Chen, C.-H.; Lee, C.-M.; Lee, G.-H.; Peng, S.-M. *J. Am. Chem. Soc.* **2000**, *122*, 488−494. Razavet, M.; Davies, S. C.; Hughes, D. L.; Pickett, C. J. *Chem. Commun.* **2001**, 847−848. Gloaguen, F.; Lawrence, J. D.; Schmidt, M.; Wilson, S. R.; Rauchfuss, T. B. *J. Am. Chem. Soc.* **2001**, *123*, 12518−12527. Lyon, E. J.; Georgakaki, I. P.; Reibenspies, J. H.; Darensbourg, M. Y. *J. Am. Chem. Soc.* **2001**, *123*, 3268−3278. George, S. J.; Cui, Z.; Razavet, M.; Pickett, C. J. *Chem.—Eur. J.* **2002**, *8*, 4037−4046. Lawrence, J. D.; Rauchfuss, T. B.; Wilson, S. R. *Inorg. Chem.* **2002**, *41*, 6193−6195. Razavet, M.; Borg, S. J.; George, S. J.; Best, S. P.; Fairhurst, S. A.; Pickett, C. J. *Chem. Commun.* **2002**, 700−701. Liaw, W.-F.; Tsai, W.-T.; Gau, H.-B.; Lee, C.-M.; Chou, S.-Y.; Chen, W.-Y.; Lee, G.-H. *Inorg. Chem.* **2003**, *42*, 2783−2788. Razavet, M.; Davies, S. C.; Hughes, D. L.; Barclay, J. E.; Evans, D. J.; Fairhurst, S. A.; Liu, X.; Pickett, C. J. *Dalton Trans.* **2003**, 586−595. Lawrence, J. D.; Li, H.; Rauchfuss, T. B.; Benard, M.; Rohmer, M.-M. *Angew Chem., Int. Ed.* **2001**, *40*, 1768−1771.

10.1021/ic049746e CCC: $27.50
Published on Web 08/11/2004

Scheme 1. Summary of the Reduction Chemistry Reported for **1**[a,7,10,14,15]

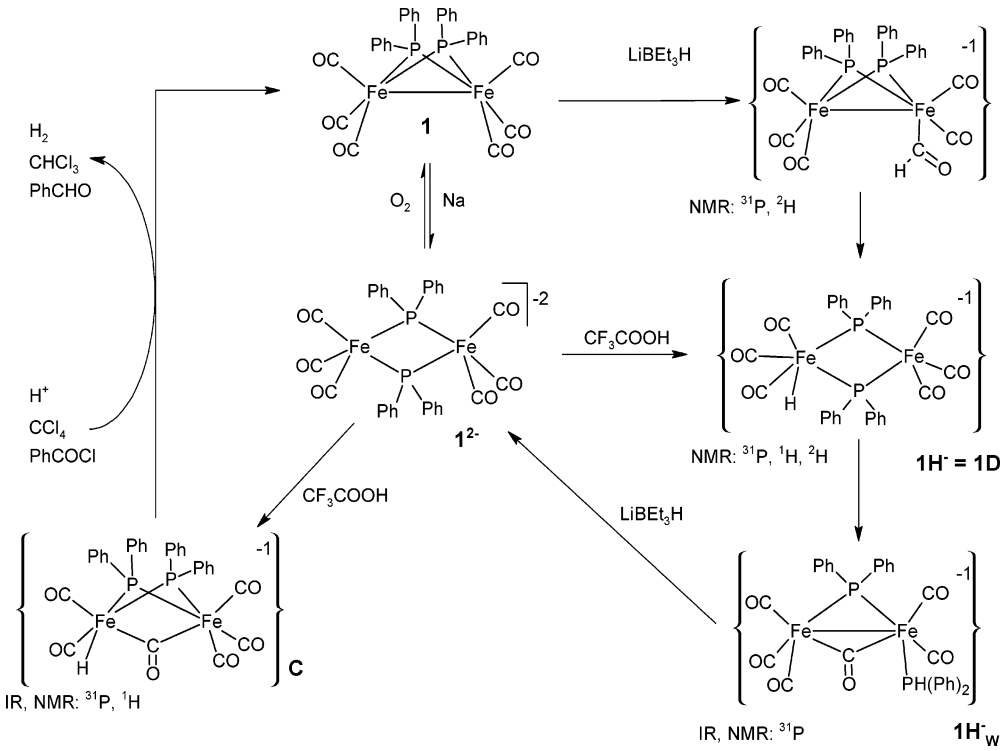

[a] X-ray structures are available for **1** and $\mathbf{1}^{2-}$;[11] in all the other cases, the type of spectroscopic evidence used to support the proposed structures is indicated.

insights gained from the study of the phosphido-bridged compounds will contribute to our understanding of the related dithiolato-bridged compounds. The close similarity of the ν(CO) bands of **C** and a product formed during the reduction of dithiolato-bridged diiron carbonyl compounds[8] supports this proposition.

Electrochemical[7,9] or chemical[7,10] reduction of **1** results in the formation of $\mathbf{1}^{2-}$, where both the neutral and reduced products have been characterized structurally.[11] For related compounds the stability of the one-electron reduced product is strongly dependent on the substituent on the phosphorus;[12,13] in the case of the diphenylphosphido bridge the monoanion is unstable with respect to disproportionation, and this is reflected by failure to observe an EPR spectrum from the reaction product of **1** and $\mathbf{1}^{2-}$. Protonation of $\mathbf{1}^{2-}$ has been the subject of studies by Collman and co-workers[7] in 1982 and Wojcicki and co-workers.[10,14,15] While the reactions conducted in the two studies are related, the reaction products obtained are spectroscopically distinct, this being reflected by the proposed structures. In neither study nor in our own work to date has either product been obtained in a form suitable for crystallographic analysis. As far as we are aware, no subsequent study has either sought to rationalize the difference in the chemistry or to confirm the structure of the reaction products. In addition to the presence of key structural features relevant to $\{2Fe2S\}_H$, **C** is also reported to undergo hydride transfer chemistry[1] as is summarized in Scheme 1. These observations suggest that **C** may serve both as a structural and functional model of $\{2Fe2S\}_H$.

In this paper we describe IR spectroelectrochemical experiments conducted under argon and carbon monoxide that lead preferentially either to **C** or $\mathbf{1H^-_W}$. These experiments have led to the identification of conditions that permit the isolation of either product, and this has permitted the collection of a broader range of spectroscopic and EXAFS results. On the basis of these studies, a revised structure for **C** is proposed. The effect of elevated proton concentration on the electrochemistry of **1** is examined, and it is shown that in the presence of sufficiently strong acids the system is electrocatalytic in terms of proton reduction. Intermediates

(3) Darensbourg, M. Y.; Lyon, E. J.; Zhao, X.; Georgakaki, I. P. *Proc. Natl. Acad. Sci. U.S.A.* **2003**, *100*, 3683−3688.
(4) Zhao, X.; Georgakaki, I. P.; Miller, M. L.; Mejia-Rodriguez, R.; Chiang, C.-Y.; Darensbourg, M. Y. *Inorg. Chem.* **2002**, *41*, 3917−3928. Gloaguen, F.; Lawrence, J. D.; Rauchfuss, T. B. *J. Am. Chem. Soc.* **2001**, *123*, 9476−9477. Georgakaki, I. P.; Miller, M. L.; Darensbourg, M. Y. *Inorg. Chem.* **2003**, *42*, 2489−2494.
(5) Gloaguen, F.; Lawrence, J. D.; Rauchfuss, T. B.; Benard, M.; Rohmer, M.-M. *Inorg. Chem.* **2002**, *41*, 6573−6582.
(6) Chong, D.; Georgakaki, I. P.; Mejia-Rodriguez, R.; Sanabria-Chinchilla, J.; Soriaga, M. P.; Darensbourg, M. Y. *Dalton Trans.* **2003**, 4158−4163.
(7) Collman, J. P.; Rothrock, R. K.; Finke, R. G.; Moore, E. J.; Rose-Munch, F. *Inorg. Chem.* **1982**, *21*, 146−56.
(8) Razavet, M. Ph.D. Thesis, University of East Anglia, Norwich, U.K., 2002. Borg, S. J.; Behrsing, T.; Best, S. P.; Razavet, M.; Liu, X.; Pickett, C. J. Manuscript in preparation.
(9) Dessy, R. E.; Kornmann, R. L.; Smith, C.; Haytor, R. *J. Am. Chem. Soc.* **1968**, *90*, 2001−4.
(10) Yu, Y. F.; Gallucci, J.; Wojcicki, A. *J. Am. Chem. Soc.* **1983**, *105*, 4826−8.
(11) Ginsburg, R. E.; Rothrock, R. K.; Finke, R. G.; Collman, J. P.; Dahl, L. F. *J. Am. Chem. Soc.* **1979**, *101*, 6550−62.
(12) Baik, M.-H.; Ziegler, T.; Schauer, C. K. *J. Am. Chem. Soc.* **2000**, *122*, 9143−9154.
(13) van der Linden, J. G. M.; Heck, J.; Walther, B.; Boettcher, H. C. *Inorg. Chim. Acta* **1994**, *217*, 29−32.
(14) Shyu, S. G.; Wojcicki, A. *Organometallics* **1985**, *4*, 1457−9.
(15) Wojcicki, A. *Inorg. Chim. Acta* **1985**, *100*, 125−33.

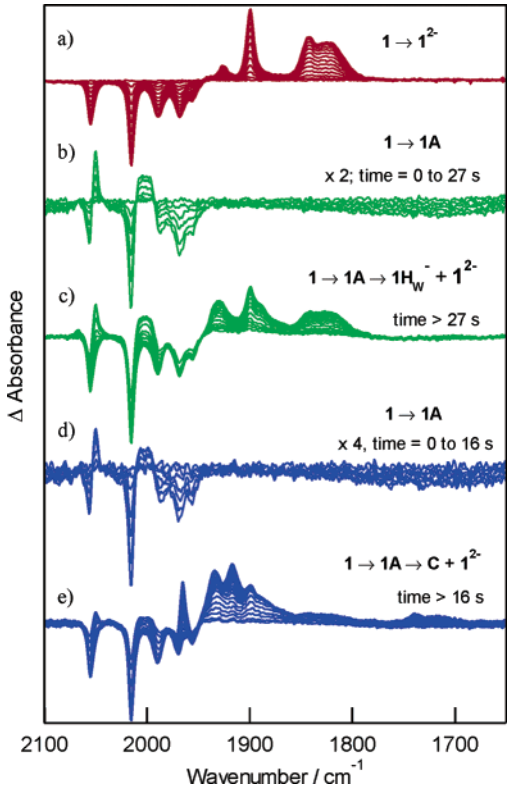

Figure 1. IR spectra in the ν(CO) region recorded during reduction of **1** (3 mM, 0.2 M (TBA)ClO_4/THF) (a) under 0.4 MPa Ar, (b, c) with HOTs (27 mM; 0.4 MPa Ar), and (d, e) with HOTs (27 mM; 0.4 MPa CO).

formed in the course of the reactions have been identified using spectroelectrochemical and continuous-flow electrosynthetic techniques, and a reaction mechanism consistent with the spectroscopic and electrochemical results is presented.

Results and Discussion

Electrochemistry and Spectroelectrochemistry (SEC) of 1. The phosphido-bridged diiron compounds, $Fe_2(\mu\text{-}PR_2)_2(CO)_6$, undergo well-defined two-electron reductions to give the corresponding dianion.[7,9] The comproportionation reactions of the neutral and dianion forms of the compound have been found to yield observable concentrations (by EPR) of the one-electron reduced product in the case where R = Me[16] but not for R = Ph.[11] The sensitivity of the disproportionation equilibrium to the identity of the R group is also reflected by density functional calculations.[12] In the course of the reduction the Fe−Fe single bond is lost and the {2Fe2P} butterfly is replaced by a planar core geometry. This structural change may be expected to contribute to a high barrier to electron transfer contributing to the value of ΔE_p (220 mV, 100 mV/s) for the two-electron reduction of **1** when using a platinum working electrode.[13] It is interesting that the reduction appears to occur in a single two-electron step when using a hanging-mercury-drop electrode (ΔE_p = 45 mV).[7] IR spectra recorded during the reduction of **1** at −1.5 V in a thin-layer SEC experiment are shown in Figure 1a.

(16) Dessy, R. E.; Rheingold, A. L.; Howard, G. D. *J. Am. Chem. Soc.* **1972**, *94*, 746−52.

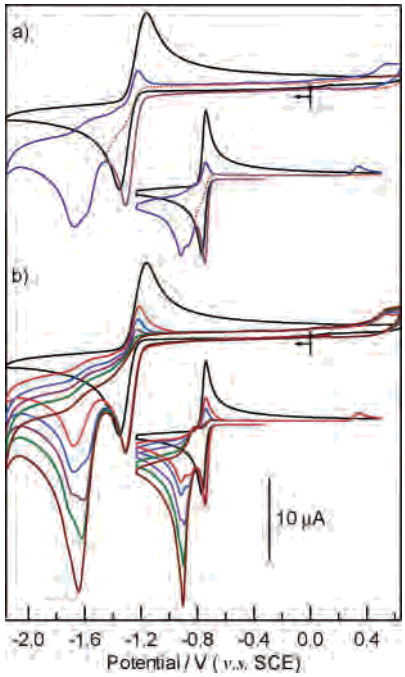

Figure 2. Cyclic voltammetry of a 1 mM solution of **1** with HOTs: (a) 0 and 2 equiv; (b) 0−5 equiv (0.2 M (TBA)PF_6/THF, ν = 100 mV s^{-1}, 0.03 cm^2 vitreous carbon working electrode). Digital simulation[18] of these experiments using the model given in Scheme 2 is given in the insets.

The spectral changes indicate a clean conversion of the starting material to a single product with no significant buildup of additional species during the course of the reaction. As expected, the spectrum of the reaction product matches that of $\mathbf{1}^{2-}$ and reoxidation of the film of solution in contact with the working electrode at a potential of −0.9 V leads to near quantitative recovery of the starting material (Supporting Information).

Whereas the reduction wave of **1** (E_{pc} = −1.4 V) is only slightly shifted to more positive potentials on addition of acid, the reoxidation wave is almost completely quenched (Figure 2). A second reduction wave is observed with $E_{pc} \approx$ −1.7 V (ν = 100 mV s^{-1}) having I_{pc} related to the concentration of acid. At lower acid concentrations this wave has two components. The absence of similar features in analogous experiments conducted on *p*-toluenesulfonic acid (HOTs) in the absence of **1** suggests that the wave at ca. −1.7 V is due to electrocatalytic proton reduction with the electrocatalyst being a protonated reduction product of **1**. Since $\mathbf{1}^{2-}$ is known to react rapidly with acids much weaker than HOTs,[14] the appearance of a reoxidation wave requires that the acid concentration be depleted near the working electrode. The appearance of a reoxidation wave when the potential is scanned more negative than −1.7 V (Figure 2) is consistent with the consumption of protons during the second reduction process.

SEC experiments of **1** in the presence of 9 molar equiv of HOTs in THF under an atmosphere of argon show clearly the involvement of an additional species, **1A**, in the initial phase of the experiment (Figure 1b). At longer times a more complex set of bands develop that may be attributed to a mixture of $\mathbf{1H}^-_\mathbf{W}$ and $\mathbf{1}^{2-}$ with a small amount of **C** that

grows into the spectrum at longer reaction times (Figure 1c). The addition of HOTs has no observable effect on the depletion bands observed inthe IR-SEC experiments, indicating that HOTs in THF is not a sufficiently strong acid to protonate **1**. The formation of $\mathbf{1}^{2-}$ in the latter stages of the reduction confirms the interpretation of the electrochemistry, i.e. that there is depletion of the acid concentration following polarization of the working electrode at potentials more negative than ca. −1.6 V. Since neither $\mathbf{1H}^{-}_{W}$ nor **C** reacts with protons to generate dihydrogen at an appreciable rate and reduction of either species requires the application of more negative potentials, it is unlikely that either $\mathbf{1H}^{-}_{W}$ or **C** is an intermediate in the catalytic proton reduction reaction. Reoxidation of the solution at −0.9 V results in the limited recovery of **1**, and this may be attributed to the reoxidation of $\mathbf{1}^{2-}$. More strongly oxidizing potentials are required to remove $\mathbf{1H}^{-}_{W}$ from the spectrum (ca. −0.5 V) although this does not lead to significant recovery of **1**.

SEC experiments of **1** in the presence of 9 molar equiv of HOTs in THF carried out under 0.68 MPa of CO *initially* yield results that are indistinguishable from those obtained under an argon atmosphere (Figure 1b,d). However, the distribution of reduction products obtained following depletion of the acid is markedly different (Figure 1c,e), where **C** is the predominant product with lesser amounts of $\mathbf{1}^{2-}$ and only trace quantities of $\mathbf{1H}^{-}_{W}$ formed. The current response observed during SEC experiments conducted under argon or CO is similar, as is the time evolution of products (including $\mathbf{1}^{2-}$). This suggests that the rate of electrocatalytic proton reduction is not affected by the relative concentrations of $\mathbf{1H}^{-}_{W}$ and **C**, supporting the argument that neither plays an important role in the catalytic cycle. The marked change in relative stability of $\mathbf{1H}^{-}_{W}$ and **C** in experiments conducted under argon and CO suggests a difference in CO stoichiometry for the two compounds. Reoxidation at a potential of −0.9 V results in conversion of $\mathbf{1}^{2-}$ into **1**. The application of a more oxidizing potential, ca. −0.2 V, results in depletion **C** with limited recovery of **1** together with another product with an IR spectrum similar to that reported for $Fe_2(\mu\text{-}PPh_2)(CO)_7$.[17]

Well-defined solutions of **1A** can be generated by continuous-flow electrosynthesis of **1**−HOTs in the mole ratio 1:3 in CH_3CN at a reduction potential of ca. −1.5 V. The electrogenerated solution of **1A** is stable with respect to further reaction with the acid, and this suggests that **1A** is the initial reduction product formed in the presence of HOTs and this is further reduced at −1.7 V in the electrochemical experiments. The IR spectra of **1** and its stable reduction products are shown in Figure 3. The ν(CO) bands of the different compounds are highly sensitive to their charge state, with the ν(CO) bands of $\mathbf{1}^{2-}$ ca. 120 cm^{-1} lower than those of **1**. The ν(CO) bands of $\mathbf{1H}^{-}_{W}$ and **C** occur at intermediate wavenumbers, consistent with their relation to **1** by $2e^-/1H^+$ reaction. The similarity of the ν(CO) bands of **1** and **1A** suggest that they share a common charge state; i.e., **1A** is related to **1** by either $1e^-/1H^+$ or $2e^-/2H^+$ reaction.

(17) Baker, R. T.; Krusic, P. J.; Calabrese, J. C.; Roe, D. C. *Organometallics* **1986**, *5*, 1506−1508.

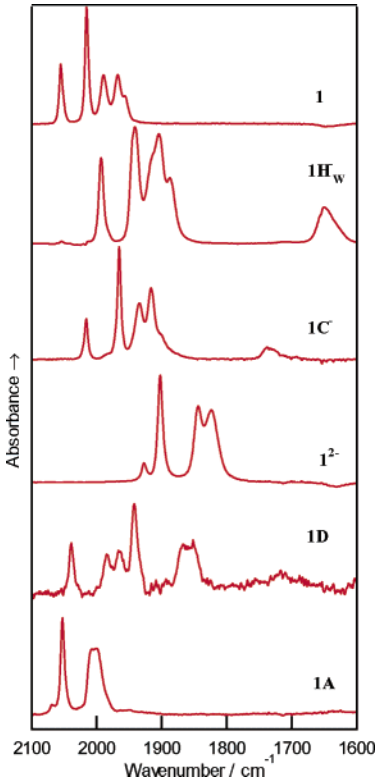

Figure 3. IR spectra in the ν(CO) region of **1** and its electrogenerated products. The spectra of **1**, $\mathbf{1H}^{-}_{W}$, and **C** were obtained from THF solutions of isolated samples. The spectra of $\mathbf{1}^{2-}$, **1A**, and **1D** were obtained from continuous-flow electrosynthesis experiments (0.2 M $(TBA)ClO_4/CH_3CN$) conducted in the presence of HOTs (**1A**) or CH_3COOH (**1D**). Whereas samples of $\mathbf{1}^{2-}$ were obtained pure, samples of **1A** and **1D** were obtained as mixtures with **1** and, in the latter case, $\mathbf{1H}^{-}_{W}$. The spectra of **1A** and **1D** were obtained by subtraction.

Scheme 2. Mechanism for Electrocatalytic Proton Reduction Used for Electrochemical Simulations[a]

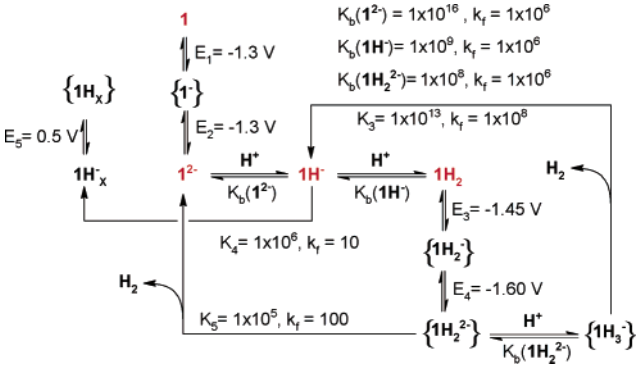

[a] In all cases common values of the diffusion coefficients (1×10^{-5} cm^2 s^{-1}), the rate of heterogeneous electron transfer (0.1 cm s^{-1}), and the α parameter (0.5) were used.

Electrochemical Simulation of the Reduction of 1. The simplest mechanism for the reduction of **1** consistent with the electrochemical and SEC results in THF in the presence of HOTs is shown in Scheme 2. This is used in digital simulations of the electrochemical experiments shown in Figure 2. While the available voltammetric results are not sufficient to permit quantitative determination of the kinetic and thermodynamic parameters, they provide a test of the validity of the proposed mechanism. To reduce the parameter space available to the simulation the diffusion coefficients

of all species were set at 1×10^{-5} cm^2 s^{-1}, the rates of heterogeneous electron transfer were set to 0.1 cm s^{-1}, and the forward rate constant for proton transfer was assumed to be fast and was arbitrarily set to 1×10^6 M^{-1} s^{-1}. No corrections have been included for the *iR* drop that is apparent for the experimental data. The remaining kinetic and thermodynamic parameters were adjusted so as to reproduce the general features of the electrochemistry for a range of acid concentrations (0−5 equiv).

The small shift of E_{pc} (ca. 20 mV) of the first reduction wave following addition of acid may, in principle, result from protonation of either of the initial reduction products, $\mathbf{1}^-$ or $\mathbf{1}^{2-}$. The calculated acid concentration dependence of the current response is in better agreement with experiment if the reduction process involves two one-electron reactions, with protonation of $\mathbf{1}^-$ uncompetitive with the second reduction step. If, as suggested by the wavenumbers of the ν(CO) bands, **1A** is in a neutral charge state, then this must be related to **1** by $2e^-/2H^+$ reaction (i.e. $\mathbf{1H_2}$). The alternative formulation of **1A**, as **1H**, would be inconsistent with Scheme 1 and can also be excluded since such a formulation would imply that protonation of $\mathbf{1}^-$ leads to a shift of the reduction potential to more negative values. This is contrary to the large shift to more positive potentials observed to accompany protonation of related compounds.[5,19] The shoulder on the wave associated with electrocatalytic proton reduction (Figure 2) implies the presence of a proton-assisted path for dihydrogen elimination. This may be modeled in an overall two-electron reduction with evolution of dihydrogen from $\mathbf{1H_2}^{2-}$ and $\mathbf{1H_3}^-$. Further investigation is needed to clarify the details of this step of the reaction. The rearrangement of $\mathbf{1H}^-$ to $\mathbf{1H_W}^-$ has previously been proposed on the basis of NMR studies of the reaction between **1** and Super-Hydride.[14,15] This interconversion is consistent with the evolution of IR spectra in the IR-SEC experiments. The formation of **C**, which occurs at longer times for experiments conducted under argon, is not modeled in Scheme 2. It is noted that a product having an oxidation potential of ca. −0.5, similar to that of $\mathbf{1H_W}^-$, is formed in cyclic voltammetric experiments conducted with less than ca. 1 equiv of acid. This wave is likely to be due to the oxidation of $\mathbf{1H_W}^-$, where at higher acid concentrations this species is protonated.[10] It is the protonated form of $\mathbf{1H_W}^-$ ($\mathbf{1H_X}^-$, Scheme 2) that is oxidized at more positive potentials.

Despite having a common charge state $K_b(\mathbf{1}^-)$ and $K_b(\mathbf{1H}^-)$ are required to be markedly different for the mechanism shown in Scheme 2. Since protonation of $\mathbf{1}^-$ is not competitive with reduction, $K_b(\mathbf{1}^-)$ must be less than ca. 1, whereas a large value of $K_b(\mathbf{1H}^-)$ is required to reproduce the reoxidation wave of $\mathbf{1}^{2-}$ obtained after electrocatalytic proton reduction (Figure 2). In this context it is critical to confirm that the stable protonated product of $\mathbf{1}^{2-}$ (i.e. **1A**) corresponds to the doubly protonated neutral species, $\mathbf{1H_2}$, as inferred

Scheme 3. Protonation Products of $\mathbf{1}^{2-}$

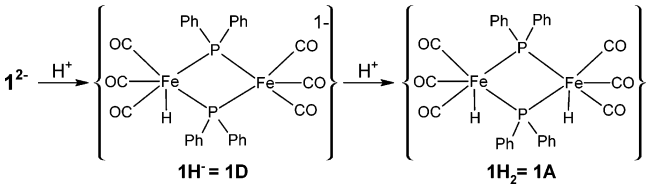

by the wavenumbers of the ν(CO) bands. This can be most clearly established by the observation of its singly protonated precursor.

The protonation reactions of the highly reactive $\mathbf{1}^{2-}$ species are most conveniently examined in mixing experiments where $\mathbf{1}^{2-}$ is generated immediately prior to reaction. This has been achieved using a continuous-flow electrosynthesis cell coupled to a mixing valve with the reaction products monitored, in-line, by IR spectroscopy. Reactions conducted in CH_3CN using 2, or more, molar equiv of HOTs result in formation of relatively stable solutions of **1A**. The addition of $\mathbf{1}^{2-}$ to 1 mol equiv of HOTs results in a more complex reaction, with transient formation of **1A** and predominant formation of $\mathbf{1H^-_W}$. Reaction between $\mathbf{1}^{2-}$ and CH_3COOH ($pK_a = 28$ in CH_3CN[20]) yields $\mathbf{1H^-_W}$ even at large molar excesses of the weak acid. IR spectra recorded from solutions immediately after mixing contain bands that are due to an intermediate species (**1D**) that subsequently rearranges to give $\mathbf{1H^-_W}$. The spectra of $\mathbf{1}^{2-}$, **1D**, and **1A** obtained in the continuous-flow experiments are shown in Figure 3.

Shyu and Wojcicki have previously reported ^{31}P, ^{2}H, and ^{1}H NMR studies of the low-temperature reduction of **1** by Super-Hydride and the protonation of $\mathbf{1}^{2-}$ by CF_3COOH. These indicate that both reactions produce $\mathbf{1H^-_W}$ and proceed through an intermediate formulated with a terminal hydride on one of the iron atoms of $\mathbf{1}^{2-}$ (Scheme 1).[14] The IR spectrum of **1D** is consistent with such a formulation, with the higher wavenumber set of ν(CO) bands (2038, 1981, and 1962 cm^{-1}) associated with the Fe(CO)$_3$ subunit at the site of protonation. Protonation of the remaining iron atom reestablishes the equivalence of the two *fac*-Fe(CO)$_3$ fragments thereby accounting for the similar pattern of bands observed for $\mathbf{1}^{2-}$ and **1A**. Thus, the intermediate **1D** and the product **1A** correspond to $\mathbf{1H}^-$ and $\mathbf{1H_2}$ in Scheme 2, where the previously reported[14] NMR spectra of $\mathbf{1H}^-$ and the IR spectra obtained in this study are consistent with the structures shown in Scheme 3. The mixing experiments conducted using CH_3COOH and HOTs suggest a much larger difference between $K_b(\mathbf{1}^{2-})$ and $K_b(\mathbf{1H}^-)$ than obtained from modeling the electrochemistry. In this regard it is noted that electrochemical modeling using Scheme 2 provides a lower limit on $K_b(\mathbf{1}^{2-})$. The involvement of a reaction pathway involving reduction of $\mathbf{1H}^-$ can be tested by the observation of electrocatalysis in acids that are insufficiently strong to protonate this species. Whereas the addition of CH_3COOH to a THF solution of **1** has a marked effect on the reversibility of the two-electron wave at −1.3 V, the presence of a large molar excess of CH_3COOH (>20-fold) does not lead to

(18) Rudolph, M.; Reddy, D. P.; Feldberg, S. W. *Anal. Chem.* **1994**, *66*, 589A−600A.
(19) Guedes da Silva, M. F. C.; Frausto da Sila, J. J. R.; Pombeiro, A. J. L.; Amatore, C.; Verpeaux, J. N. *NATO ASI Ser., Ser. C* **1993**, *385*, 483−7.
(20) Izutsu, K. *Acid-Base Dissociation Constants in Dipolar Aprotic Solvents*; Blackwell Scientific Publications: Oxford, U.K., 1990.

significant proton reduction or to a reduction process attributable to $\mathbf{1H}^-$ at potentials more positive than −2.3 V. This observation confirms the assignment of the reduction wave with $E_{pc} \approx -1.7$ V to a process involving $\mathbf{1H_2}$ and permits the exclusion of mechanisms involving reduction of $\mathbf{1H}^-$.

The failure of $\mathbf{1}^{2-}$ to reduce protons and yield dihydrogen when HOTs is used as the acid may be understood in terms of a structure in which there is a planar {2Fe2P} core and the two $FeH(CO)_3$ centers interact weakly. While a folding of the core may be expected to facilitate elimination of dihydrogen with recovery of **1**, it would appear that this reaction does not proceed at an appreciable rate prior to further reduction. Paradoxically, reaction of $\mathbf{1}^{2-}$ with the weaker acid CF_3COOD is reported to give D_2 in high isotopic purity.[7] In this case the acid is insufficiently strong to generate **1A** and rearrangement of $\mathbf{1H}^-$ leads to the formation of a product that is able to act as a hydride donor. It is clear from the electrochemistry (Figure 2) that this reaction is slow compared with electrocatalysis associated with reduction of **1A**.

Formulation of C. The differences in the SEC experiments of **1** in the presence of a proton source under an atmosphere of argon or CO suggest that **C** may be formed cleanly from reactions conducted using CO-saturated solvents. Indeed **C** can be obtained by saturating a solution of $\mathbf{1H}^-_\mathbf{W}$ with CO, this being the basis of an alternative method for its preparation. Despite repeated attempts **C** was not obtained in a form suitable for X-ray structural analysis and its structure remains to be established. ESI-MS experiments conducted on dilute solutions of **C** yielded, at low cone voltages (5 V), a parent peak with *m*/*z* centered on 493 with an isotopic distribution consistent with a monoanion of formulation $[Fe_2(PPh_2)(CO)_7]^-$. At higher cone voltages (30−50 V) increasing numbers of CO groups are fragmented from the molecular ion (Supporting Information). In no experiment was there any indication of the presence of an ion with $m/z = 651$ as would be expected for the structure proposed for **C** (Scheme 1). Analogous experiments conducted on $\mathbf{1H}^-_\mathbf{W}$ yielded parent peaks centered on $m/z = 493$ and 651, where the relative intensities of the two peaks varied between experiments. The isotopic distribution of the peaks centered on $m/z = 651$ match that required for the proposed structure.

The ^{1}H and ^{31}P NMR of isolated samples of **C** yield resonances consistent with there being a single phosphorus environment.[7] Solutions of **C** prepared by CO saturation of $\mathbf{1H}^-_\mathbf{W}$ yield IR spectra indistinguishable from those of isolated **C**; however, additional ^{1}H (multiplets centered on 7.34 and 7.52 ppm) and ^{31}P (singlet at −41 ppm in proton decoupled spectra) resonances are observed and these are consistent with their assignment to diphenylphosphine.[21] The relative intensities of these resonances are less than those of the PPh_2^- group of **C**, whereas a 1:1 ratio is expected if conversion of $\mathbf{1H}^-_\mathbf{W}$ to **C** involves the loss of $PHPh_2$. This difference may be explained in terms of the volatility of the free phosphine where solutions prepared by CO saturation of $\mathbf{1H}^-_\mathbf{W}$ are marked by a strong "phosphine" odor.

Table 1. Comparison of Spectroscopic Data for **C** and That Reported for $[Fe_2(\mu\text{-}PPh_2)(\mu\text{-}CO)(CO)_6]^-$, **2**

	[(15C5)Li]**C**[a]	[NEt$_4$]**2**[b]		PPN**2**[c]
IR[d]/cm^{-1}	THF	THF	Nujol	Nujol
	2015 (ms)	2010 (m)	2010 (s)	2016 (vs)
	1965 (vs)	1965 (vs)	1965 (s)	1964 (vs, br)
	1916 (s)	1935 (s)	1910 (s, br)	1928 (s)
	1904 (w, sh)	1920 (s)		1904 (w)
			1865 (s)	1892 (w)
	1733 (w, br)	1705 (w, br)	1735 (s, br)	1724 (vs)
NMR, ^{1}H/δ	7.31 (mpt, 2H)			7.21−7.8 (mpt)
	7.61 (mpt, 3H)			
NMR, ^{31}P{H}[e]/δ	127 (CD_3CN)			125.3 (CH_2Cl_2)

[a] This work. [b] Reference 22. [c] Reference 23. [d] s = strong, m = medium, w = weak, vs = very strong, sh = shoulder, br = broad, mpt = multiplet. [e] Relative to H_3PO_4.

Following an earlier study,[24] two crystallographic reports of diiron carbonyl compounds having a single bridging phosphido group have previously been published.[22,23] These include the anion $[Fe_2(\mu\text{-}PPh_2)(\mu\text{-}CO)(CO)_6]^-$, **2**, and the method of preparation involved reaction of $[Fe_2(CO)_8]^{2-}$ with PR_2Cl followed by decarbonylation. The reported spectroscopic details (IR, NMR) are consistent with those obtained for the sample of **C** (Table 1), and the structural parameters are clearly consistent with the presence of an Fe−Fe bond (Table 2). Despite the strong support for the assignment of the structure of **C** to **2** provided by the ESI-MS and spectroscopic details the report that the ^{1}H NMR of **C** includes a triplet ($J_{HP} = 42.5$) at $\delta = -20$ together with hydridic reactions with protons, benzoyl chloride, and carbon tetrachloride[7] are inconsistent with such a structure.

The formation of **C** by reaction of $\mathbf{1H}^-_\mathbf{W}$ and CO may proceed by substitution of the terminal $PHPh_2$ group, in which case the 34 electron diiron product would retain the Fe−Fe bond whereas addition of CO to $\mathbf{1H}^-_\mathbf{W}$, or CO-mediated rearrangement of $\mathbf{1H}^-_\mathbf{W}$ to the structure proposed for **C** (Scheme 1), would give a product without an Fe−Fe bond. Thus, the Fe−Fe separation provides an additional means of distinguishing between the different structures proposed for **C**. In the absence of a crystalline sample metric details of the Fe−Fe separation can be obtained from the application of EXAFS techniques. Iron K-edge X-ray fluorescence spectra were obtained from solutions of **1**, $\mathbf{1}^{2-}$, $\mathbf{1H}^-_\mathbf{W}$, and **C** and solid-state samples of **1** diluted in boron nitride. In these experiments the integrity of the electrochemically ($\mathbf{1}^{2-}$) and chemically ($\mathbf{1H}^-_\mathbf{W}$ and **C**) generated samples was confirmed by in-line IR measurements collected immediately prior to freezing the solution at 80 K.

The models used to refine the EXAFS data are summarized in Table 2. In all cases the number of refined parameters was minimized while still allowing the main features of the proposed structures to be represented. A discussion of the alternate strategies for modeling the EXAFS results for diiron

(21) Emsley, J.; Hall, D. *The Chemistry of Phosphorus*; John Wiley & Sons: New York, 1976.

(22) Ellis, J. E.; Chen, Y.-S. *Organometallics* **1989**, *8*, 1350−1361.

(23) Walther, B.; Hartung, H.; Bottcher, H.-C.; Baumeister, U.; Bohland, U.; Reinhold: J.; Sieler, J.; Ladriere, J.; Schiebel, H.-M. *Polyhedron* **1991**, *10*, 2423−2435.

(24) Osterloh, W. T. Ph.D. Thesis, University of Texas, Austin, TX, 1982; University Microfilms International: Ann Arbor, MI, 1982

Table 2. Summary of the EXAFS Refinements of **1**, $\mathbf{1}^{2-}$, $\mathbf{1H}^{-}_{\mathbf{W}}$, and **C**[a]

	sample[b]				
	1 (solid)	**1**	$\mathbf{1}^{2-}$	$\mathbf{1H}^{-}_{\mathbf{W}}$	**C**
model[c]	M1	M1	M1	M2	M3
k/Å^{-1}	1−15	1−15	1−14	1−14.5	1−14
R/Å	0.75−3.8	0.75−3.8	0.75−4	0.75−3	0.75−3
E_0/eV	−9.02	−7.24	−8.39	−7.33	−5.68
S_0^2	0.73	0.73	0.95	0.91	0.91
χ^2 [R_{XAFS} (%)][d]	3.84 [17.5]	5.59 [17.4]	3.33 [15.0]	0.57 [8.1]	1.49 [13.2]
Fe−Fe/Å[e]	2.61 [2.630][f]	2.61	3.58 [3.63][g]	2.58	2.59 [2.601][h]
	(0.0025)	(0.0007)	(0.0060)	(0.0034)	(0.0043)
Fe−P/Å	2.21 [2.212]$_{av}$	2.21	2.26 [2.29]	2.17	2.18 [2.209]$_{av}$
	(0.0028)	(0.0009)	(0.0034)	(0.0010)	(0.0019)
Fe−C/Å	1.78 [1.781]$_{av}$	1.78	1.75 [1.75]	1.77	1.78 [1.777]$_{av}$
	(0.0010)	(0.0006)	(0.0026)	(0.0031)	(0.0053)
C−O/Å	1.16 [1.140]$_{av}$	1.15	1.17 [1.15]	1.15	1.16 [1.144]$_{av}$
	(0.0023)	(0.0021)	(0.0036)	(0.0036)	(0.0047)
Fe−$C_{\alpha/b}$/Å	3.52 [3.543]$_{av}$	3.52	3.50 [3.45]	2.25	2.13 [1.962]$_{av}$
	(0.0027)	(0.0018)	(0.0035)	(0.0047)	(0.0010)
C−O_b/Å				1.12	1.31 [1.176]$_{av}$
				(0.0010)	(0.0010)
Fe−P_t/Å				2.23	
				(0.0012)	

[a] Fits of the EXAFS data in k and R space are included in the Supporting Information. [b] Unless otherwise stated data were collected from 3 to 5 mM solutions in acetonitrile (**1** and $\mathbf{1}^{2-}$) or THF ($\mathbf{1H}^{-}_{\mathbf{W}}$ and **C**). [c]

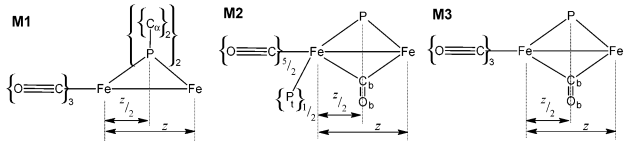

[d] $\chi^2 = \int_{k=0...\infty}[w(\chi_{obs}(k) - \chi_{calc}(k))]^2$, $R_{XAFS} = \int_{k=0...\infty}[\chi^2/\chi^2_{calc\equiv 0}]^{1/2}$; $\chi_{obs}(k)$ and $\chi_{calc}(k)$ are the observed and calculated EXAFS and w is a weighting factor.[27] [e] Crystallographic distances are given in brackets, and the Debye Waller factors, in parentheses. The errors in the internuclear contacts is dominated by the typical systematic error, assigned a conservative consensus value of 0.02.[28] [f] Fe−Fe and Fe−P are available for **1**;[11] other bond distances were obtained from $Fe_2(\mu\text{-PhP}(CH_2)_3PPh_2)(CO)_6$.[29] [g] $[NEt_4]_2\mathbf{1}^{2-}$.[11] [h] $[NEt_4]_2\mathbf{2}$.[22]

carbonyl compounds of this sort is included in a separate publication.[25] Good internal consistency of the data was obtained for repeated measurements of the same compound and, in the case of **1**, for samples measured in the solid and solution state. In all cases the determinancy of the fit was good, with the ratio of the number of refined parameters to the number of independent points[26] ranging between 1.3 ($\mathbf{1H}^{-}_{\mathbf{W}}$) and 2.4 (**1**), and the refinement statistics were satisfactory in all cases. The S_0^2 and the Debye−Waller factors refined to give physically reasonable values, the exception being the somewhat low values of the Debye−Waller factors obtained for the Fe−Fe and Fe−C interactions for solutions of **1**. There is excellent agreement between the bond lengths obtained from EXAFS analysis of both **1** and $\mathbf{1}^{2-}$ and the reported crystallographic determinations (Table 2). It is noteworthy that even the long nonbonding Fe−Fe distance of $\mathbf{1}^{2-}$ is obtained with good accuracy.

Modeling the EXAFS data of $\mathbf{1H}^{-}_{\mathbf{W}}$ and **C** is complicated by the absence of an unequivocal structural assignment, and therefore, conclusions drawn from this analysis need to be model independent. In cases where the backscattering atom is significantly different in atomic number from the other scattering atoms, then the calculated internuclear separation will be largely insensitive to the details of the model. This situation applies for the backscattering iron atom, and a similar Fe−Fe separation is obtained from analysis of the EXAFS data from $\mathbf{1H}^{-}_{\mathbf{W}}$ and **C** using any of the three models described in Table 2 or for a model based on the structure of **C** given in Scheme 1. On this basis the Fe−Fe distance is determined with a high level of certainty. The Fe−Fe distances obtained for $\mathbf{1H}^{-}_{\mathbf{W}}$ and **C** are similar and are marginally shorter than that obtained for **1**. This observation is consistent with the proposed structure for $\mathbf{1H}^{-}_{\mathbf{W}}$; however, the presence of an Fe−Fe bond for **C** is inconsistent with the earlier proposed structure and is in excellent agreement with that expected for structure **2**. Moreover, the structural parameters obtained from the analysis of **C** are in excellent agreement with the crystallographic values obtained from $[NEt_4]\mathbf{2}$ (Table 2).

The reported hydride transfer properties of **C** are hard to reconcile in terms of the revised structure, i.e. **2**. It is significant that in those studies **C** was generated in situ by reaction of $\mathbf{1}^{2-}$ with 1 equiv of protons and, accordingly, the solutions would have contained both **2** and $PHPh_2$.[7] In the absence of $PHPh_2$ isolated samples of **C** react with protons yielding a complex mixture of products that do not include significant concentrations of **1**. Moverover, experiments in which an isolated sample of **C** is reacted with protons in the presence of thiophenol yield a product with ν(CO) bands intermediate between those of **1** and the bis-(thiophenolato)-bridged analogue. A possible explanation of

(25) Bondin, M. I.; Borg, S.; Foran, G.; Best, S. P. Manuscript in preparation.
(26) Stern, E. A. *Phys. Rev. B: Condens. Matter* **1993**, *48*, 9825−9827.

the hydride transfer chemistry attributed to **C** is that this proceeds through a hydridic species in equilibrium with **2** and $PHPh_2$. A species of structure similar to that originally proposed for **C** (Scheme 1) is an attractive candidate. Investigations into the details of this aspect of the chemistry are in progress.

Conclusions

A combination of chemical and electrosynthetic techniques have permitted identification of the intermediates formed in the course of electrocatalytic proton reduction by **1**, and this together with digital simulation of the voltammetry suggest the reaction mechanism shown in Scheme 2. Protonation of $\mathbf{1}^{2-}$ proceeds via attack at one of the iron atoms of the planar {2Fe2P} core, and this product is either protonated to give a relatively stable product, **1A** or rearranges to give $\mathbf{1H^-_W}$. The structure of $\mathbf{1H^-_W}$ previously proposed by Wojcicki[10] is consistent both with the spectroscopic results and the structural parameters obtained from EXAFS analysis. Differences in the product distribution obtained in SEC experiments of **1**−HOTs conducted under argon or CO suggest that CO replaces the terminally bound $PHPh_2$ group to give **2**. This formulation of the product is consistent with results obtained by ESI-MS and a range of spectroscopic techniques. The alternative formulations of **C** differ in terms of the number of diphenylphosphido bridging groups, which leads to differences in the Fe−Fe bonding. This aspect of the structure has been probed by a series of EXAFS measurements conducted on **1**, together with electrochemically and chemically generated samples of $\mathbf{1}^{2-}$, $\mathbf{1H^-_W}$, and **C**. While the extent of the data obtained from these measurements is insufficient to permit unambiguous structure characterization, the Fe−Fe separation is obtained with high reliability and this clearly indicates the presence of an Fe−Fe bond for **1**, $\mathbf{1H^-_W}$, and **C**. These results confirm that the previously proposed structure for **C** (Scheme 1)[7] is not tenable and all the structural parameters are in close agreement with those expected for the revised structure, **2**.

Contrary to observations for the thiolato-bridged analogue, where turnover occurs following two-electron reduction,[6] $\mathbf{1}^{2-}$ reacts with HOTs to give a doubly protonated product, **1A**, that is stable with respect to dihydrogen evolution. Further reduction is required to achieve dihydrogen elimination at a significant rate. No significant electrocatalytic proton reduction is evident for solutions of **1**−HOTs in THF following two-electron reduction. Whereas isolated samples of **C** do not act as a source of H^-, the observation of hydridic chemistry from $\mathbf{1}^{2-}$−CF_3COOH mixtures[7] suggests that one, or more, of the rearrangement products are hydridic in character. Further work is needed to delineate the chemistry of the system so as to better understand the impact of structural and electronic factors on the hydridic chemistry of phosphido- and thiolato-bridged diiron compounds.

A key aspect of the chemistry of $\{2Fe2S\}_H$ is the change in the mode of CO coordination with redox state and the coupling of this structural change to the catalytic cycle. The conversion of $\mathbf{1H^-}$ into $\mathbf{1H^-_W}$ ultimately involves such a transformation, although it is not clear whether the change in mode of CO coordination is kinetically important. The comparative inertness of $\mathbf{1H_2}$ is interesting given that the isomer $[FeH(CO)_3(\mu\text{-}PPh_2)Fe(PHPh_2)(CO)_3]$ may be formed in reactions between CF_3COOH and $\mathbf{1H^-_W}$.[10] While the structures of the protonated products of $\mathbf{1}^{2-}$ are unlikely to be as closely related to the structure of $\{2Fe2S\}_H$ as suggested by the previously proposed structure of **C**, the system exhibits remarkably well-behaved electrocatalytic proton reduction behavior that, in THF, is amenable to detailed analysis. The framework provided by such an analysis is relevant to the corresponding reactions of a broader range of bridged diiron compounds.

Experimental Section

Chlorodiphenylphosphine (PPh_2Cl) and Super-Hydride ($LiBEt_3H$, 1 M in THF) were obtained from Aldrich and used without further purification; iron pentacarbonyl was dried over calcium hydride, vacuum distilled, and stored at 4 °C under dinitrogen before use. Solvents were purified using standard procedures[30] and distilled under a dinitrogen atmosphere. Tetrahydrofuran (THF) was distilled from sodium/benzophenone, acetonitrile from CaH_2, and *n*-hexane from freshly pressed sodium wire. Unless stated otherwise, all reactions were carried out under an inert dinitrogen atmosphere using standard Schlenk techniques or conducted within a glovebox (Vacuum Atmospheres). Tetra-*n*-butylammonium perchlorate ((TBA)ClO_4) and tetra-*n*-butylammonium hexafluorophosphate ((TBA)PF_6) used as supporting electrolytes were prepared and purified using standard methods.[31] Literature methods were employed to prepare $Fe_2(\mu\text{-}PPh_2)_2(CO)_6$, **1**,[7] $[Li(15\text{-crown-}5)][Fe_2(\mu\text{-}PPh_2)(\mu\text{-}CO)(PHPh_2)(CO)_5]$, $[Li(15C5)]\mathbf{1H^-_W}$,[10] and $Na_2[Fe_2(\mu\text{-}PPh_2)_2(CO)_6]^{2-}$, $Na_2\mathbf{1}^{2-}$.[7]

Caution! *Perchlorate salts are potentially explosive. Solutions containing (TBA)ClO_4 as supporting electrolyte should not be allowed to evaporate to dryness.*

$[Li(15\text{-crown-}5)][Fe_2(\mu\text{-}PPh_2)(\mu\text{-}CO)(CO)_6]$, [Li(15C5)]**C**, was prepared by the following method. A solution of **1** in THF (0.025 g, 38.5 μmol) was treated with 1 equiv of $LiBEt_3H$ (38.5 μL, 1 M) to yield a red solution of $\mathbf{1H^-_W}$ in greater than 90% purity (IR). The solution was then saturated with CO and allowed to stand overnight. A stoichiometric quantity of 15-crown-5 ether was added, and following the addition of *n*-hexane, the crude product was isolated as a deep-red oil. The product was washed with *n*-hexane (3 × 1 mL) to remove traces of **1** to yield a spectroscopically clean sample of [Li(15C5)]**C**. IR (THF): 2015, 1965, 1934, 1916, 1733 cm^{-1}. The elemental analysis, while poor, confirmed an Fe:P ratio of at least 2:1. Anal. Calcd for $Fe_2PC_{29}H_{30}O_{12}Li$: C, 48.8; H, 4.2; Fe, 15.5; P, 4.3. Found: C, 50.05; H, 6.07; Fe, 12.6; P, 2.7.

Electrochemical measurements were conducted using either an Autolab PGSTAT30 or a MacLab potentiostat. In the former case the potentiostat was controlled using GPES software (Autolab); in the latter case EChem software with a PowerLab interface (AD-Instruments) was used. Experiments employed a standard three-electrode geometry with a 2 mm diameter vitreous carbon disk as the working electrode, a platinum gauze counter electrode, and a

(27) Ellis, P. J.; Freeman, H. C. *J. Synchrotron Radiat.* **1995**, *2*, 190−195.
(28) Gurman, S. J. *J. Synchrotron Radiat.* **1995**, *2*, 56−63.
(29) Reingold, A. L. *Acta Crystallogr., Sect. C: Cryst. Struct. Commun.* **1985**, *41*, 1043.
(30) Armarego, W. L. F.; Perrin, D. D. *Purification of Laboratory Chemicals*, 4th ed.; Butterworth-Heinemann: Oxford, U.K., 1996.
(31) Sawyer, D. T.; Sobkowiak, A.; Roberts, J. J. L. *Electrochemistry for Chemists*, 2nd ed.; Wiley-Interscience: New York, 1995.

jacketed silver wire pseudo-reference electrode. The potential of the silver electrode was referenced against the ferrocenium/ferrocene couple, and all potentials are reported relative to the saturated calomel electrode (SCE), where in THF $E^{\circ\prime}(Fc^+/Fc) = 0.53$ V.[32] The working electrode was polished with 0.3 μm alumina and sonicated in THF between experiments. Acid titration experiments were performed by measured addition of a THF solution of *p*-toluenesulfonic acid (0.2 M) together with the complex and supporting electrolyte at the same conditions as used in the initial electrochemical experiment. Electrochemical simulations were performed using DIGISIM version 3.0.[18]

Infrared spectroelectrochemical (IR-SEC) measurements were made using a purpose built high-pressure SEC cell capable of operating at elevated gas pressure.[33] In all experiments vitreous carbon was used as the working electrode. Measurements were generally conducted at gas pressures in the range 275−680 kPa. Spectra of the thin film of solution (10−20 μm) in contact with the working electrode were recorded during electrolysis at 1−2 s intervals. Spectra are presented in absorbance mode where the reference spectrum was recorded immediately before the application of an oxidizing or reducing potential. A PAR model 362 potentiostat was used to control the potential during SEC experiments.

Continuous-flow electrosyntheses were performed using a purpose built airtight cell based on a design reported previously.[34] The working and counter electrodes were fashioned from reticulated vitreous carbon, and the reference electrode consisted of a jacketed silver wire or a no-leak Ag/AgCl reference electrode (Cypress Systems), which was inserted into a small cavity in the working electrode. Standard liquid chromatography valves, gastight syringes, and fittings (Hamilton) in conjunction with thick-walled 1/16 in. Teflon tubing permitted anaerobic transfer of solution to and from the cell. The flow of solution to the cell was controlled using a syringe pump that was typically operated at a flow rate of 5 μL s^{-1}. The cell was jacketed, and the temperature could be maintained at −50 °C for the duration of the experiment. IR spectra were collected using a Bio-Rad FTS 175C spectrometer which utilized a glowbar source, Ge/KBr beam splitter, and a liquid-nitrogen-cooled MCT detector. NMR spectra were recorded using a Varian Unity Plus 400 MHz instrument; chemical shifts of ^{31}P NMR spectra were referenced relative to H_3PO_4. Electrospray mass spectra were recorded using a Micromass Quattro II mass spectrometer in negative ion mode. Deoxygenated acetonitrile was used as the mobile phase, and N_2, as the drying and nebulizing gas. Sample concentrations were approximately 0.4 μM.

X-ray fluorescence measurements were made at a temperature of ca. 10 K using beamline 20B (bending magnet) at the KEK Photon Factory, Tskuba, Japan. A channel-cut Si(111) monochromator provided an energy resolution ($\Delta E/E$) of ca. 2.4×10^{-4}, and higher order harmonics of the selected wavelength were rejected by detuning the monochromator by a factor of a half. EXAFS measurements were conducted at the Fe K-edge (7111.2 eV). Solid samples were dispersed in boron nitride, and data were measured in transmission mode using an ion chamber detector. Solutions were measured in fluorescence mode using a 10-element Ge detector and were prepared so as to give a concentration of 3−5 mM (i.e. 6−10 mM in iron) in either acetonitrile or THF. The fluorescence cell consisted of a Teflon block with a $1.5 \times 1.5 \times 10$ mm channel, and the front window consisted of a 25 μm thick film of Teflon-coated Kapton. The 1/16 in. Teflon tubing used to transfer solutions to/from the cell were press-sealed into holes in the Teflon block. For electrochemically generated samples $(TBA)PF_6$ (0.2 M) was used as the supporting electrolyte. For solutions in acetonitrile the data were in some instances affected by crystallinity leading to the loss of data over a narrow *k* range for different of the detector elements. This problem was ameliorated by rapidly freezing the sample in isopentane (140 K) before storage in liquid nitrogen prior to loading into the closed-cycle helium Displex cryostat (10 K). The quality of the samples was established by IR spectroscopy (Shimadzu Prestige FTIR) using an in-line system that included both the fluorescence EXAFS cell and a solution IR cell. The sample was frozen immediately after transfer to the EXAFS cell.

The solution sample of $\mathbf{1}^{2-}$ was generated by continuous-flow electrosynthesis.[34] The potential for these experiments was controlled using a PAR 273A potentiostat. Samples of $\mathbf{1H^-_W}$ and **C** were generated chemically. The sample of $\mathbf{1H^-_W}$ was prepared by reaction of a 3.5 mM solution of **1** in THF with 1 mol equiv of Super-Hydride. IR spectroscopy was used to confirm that the reaction proceeded quantitatively and with no significant formation of side products. Exposure of this sample to CO resulted in its conversion to **C**. Owing to the presence of Li^+ the product contains a mixture of ion-paired (35%) and non-ion-paired (65%) forms of **C**. The sample used for EXAFS measurements contained a total of 5−10% **1** and $\mathbf{1H^-_W}$ (IR, Supporting information).

Data reduction of experimental X-ray absorption spectra was performed using the program XFIT.[27,28] The photon energy was calibrated against the absorption edge of Fe foil, where the peak in the first derivative was assigned an energy of 7111.2 eV. Background removal from the EXAFS data was performed both automatically and manually using the AUTOBK algorithm[35] (implemented within Athena[36]) and XFIT[27,28] spline packages, respectively. The use of both approaches provided an additional check on the reliability of the EXAFS function.[35,37] The model structures were refined using the software package XFIT,[27,28] which incorporates ab initio FEFF 6.01[38] MS curved-wave calculations. The calculations included MS paths with $R_{max} = 4$ Å (maximum effective path length of 8 Å) and up to four legs. The plane wave and curved wave path filter thresholds were set at 2% and 3% of the strongest MS path, respectively. A nonlinear least-squares fitting is used to vary the model and concurrently optimize the fit of the calculated to the observed EXAFS.[27] The goodness of fit residual parameter (R_{XAFS}) has been defined[28] where an R_{XAFS} value around 20% is considered a good fit to the non-Fourier-transformed data, while an R_{XAFS} value greater than 40% is poor. The random (statistical) errors (σ_r) in the Fe−L bond lengths due to noise in the EXAFS data were estimated by Monte Carlo calculations.[27,28] These were combined with the typical systematic errors (σ_s), assigned a conservative consensus value of 0.02 Å,[28] to give the maximum root-mean-square (rms) error ($[\sigma_r^2 + \sigma_s^2]^{1/2}$). A description of the models used for data analysis together with details of the symmetry constraints and restraints on E_0, S_0^2, and σ^2 is available as Supporting Information.

(32) Chang, D.; Malinski, T.; Ulman, A.; Kadish, K. M. *Inorg. Chem.* **1984**, *23*, 817−24. Connelly, N. G.; Geiger, W. E. *Chem. Rev.* **1996**, *96*, 877−910.
(33) Borg, S. J.; Best, S. P. *J. Electroanal. Chem.* **2002**, *535*, 57−64.
(34) Bondin, M. I.; Foran, G.; Best, S. P. *Aust. J. Chem.* **2001**, *54*, 705−709.
(35) Newville, M.; Livins, P.; Yacoby, Y.; Rehr, J. J.; Stern, E. A. *Phys. Rev. B: Condens. Matter* **1993**, *47*, 14126−14131.
(36) Ravel, B. *Athena*, 0.8.019; University of Washington: Seattle, WA, 2001.
(37) Bridges, F.; Booth, C. H.; Li, G. G. *Physica B (Amsterdam)* **1995**, *208, 209*, 121−124. Li, G. G.; Bridges, F.; Booth, C. H. *Phys. Rev. B: Condens. Matter* **1995**, *52*, 6332−6348.
(38) Zabinsky, S. I.; Rehr, J. J.; Ankudinov, A.; Albers, R. C.; Eller, M. J. *Phys. Rev. B: Condens. Matter* **1995**, *52*, 2995−3009.

Acknowledgment. We thank Professor Chris Pickett for many insightful discussions throughout this investigation. S.P.B. gratefully acknowledges the Australian Research Council for funding this research. S.J.B. and M.I.B. acknowledge the receipt of an Australian Postgraduate Research Award. The EXAFS experiments were performed at the Australian National Beamline Facility with support from the Australian Synchrotron Research Program, which is funded by the Commonwealth of Australia under the Major National Research Facilities Program. We thank Dr. Garry Foran for expert assistance with the EXAFS experiments.

Supporting Information Available: Spectroelectrochemical plots, tables of model parameters, a description of the models, EXAFS and FT plots, and a description of EXAFS sample preparation with IR spectra. This material is available free of charge via the Internet at http://pubs.acs.org.

IC049746E